

Autodetachment spectroscopy and dynamics of dipole bound states of negative ions: ${}^2A_1 \leftarrow {}^2B_1$ transitions of H_2CCC^-

K. Yokoyama, Gary W. Leach,^{a)} Joseph B. Kim, and W. C. Lineberger
JILA, University of Colorado and National Institute of Standards and Technology, and Department of Chemistry and Biochemistry, University of Colorado, Boulder, Colorado 80309-0440

(Received 27 June 1996; accepted 23 September 1996)

The H_2CCC^- ion is studied by autodetachment spectroscopy in a coaxial laser-ion beam spectrometer. Sharp resonances at photon energies near the photodetachment threshold energy are ascribed to a ${}^2A_1 \leftarrow {}^2B_1$ transition followed by autodetachment of the dipole-bound state (DBS). Some 2500 rotational transitions are assigned and the band origin is determined to be $14\,284.420(5)$ cm^{-1} . The observation of individual rotational lines allowed determination of the rotational spectroscopic constants as $A=9.651\,53(4)$ cm^{-1} and $(B+C)/2=0.346\,461(3)$ cm^{-1} for the DBS as well as the spin-rotation coupling constant $\epsilon_{aa}=2.17(6)\times 10^{-3}$ cm^{-1} . Based on an electron affinity of $14\,469\pm 64$ cm^{-1} , the binding energy of the electron in the DBS is 170 ± 50 cm^{-1} . Anomalous rotational line positions are found in the vicinity of $K_a=7-10$ in the DBS and have been attributed to the centrifugal distortion couplings caused by mixing with the CCC out-of-plane bending mode (ν_6) and the CCC in-plane bending mode (ν_9). The linewidths provide information about autodetachment rates that make it possible to obtain electron detachment dynamics for individual rotational states. © 1996 American Institute of Physics. [S0021-9606(96)02248-9]

I. INTRODUCTION

It is a general feature of most light negative ions that they do not possess excited valence states at or below the energy required to remove the excess electron. As a result, obtaining detailed structural information about negative ions through high resolution (bound-bound) spectroscopy is sometimes difficult or impossible. While valence excited states of negative ions are uncommon, the observation¹⁻⁹ of dipole-bound electronically excited states (DBS) of anions greatly expands the scope of ions accessible to bound-bound, high resolution spectroscopic investigation. A molecule with a dipole moment greater than ~ 2 D can possess an electron bound in the $1/r^2$ electron-dipole potential and produce a "Rydberg-type" dipole-bound state (DBS). In a DBS, the electron is typically bound to the positive end of a molecular dipole by less than 10 meV (~ 80 cm^{-1}) and resides in a very diffuse orbital. This DBS is structurally similar to the neutral core, much like a Rydberg state, but unlike Rydberg states, only one or a very few of these dipole-bound electronic states are stable for each dipolar neutral molecule. Excitation of the DBS with sufficient rotational and/or vibrational energy will result in autodetachment (via rotation/vibration \rightarrow electronic coupling) to produce a radical plus a free electron. High resolution autodetachment spectroscopy of dipole-bound states is, therefore, a valuable tool with which to obtain structural information concerning negative ions and neutral radicals.

In the past, several anions were confirmed to support a DBS.¹⁰⁻¹³ We have been carrying out extensive investigations of DBS of small molecules through high resolution autodetachment spectroscopy (~ 30 MHz) utilizing a coaxial

ion/laser beam geometry.¹⁴ By measuring bound-bound transition energies and linewidths, we obtain both structural and dynamical information on the DBS through autodetachment spectroscopy. Autodetachment rates can be probed on a timescale of 5 ns to 1 ps with respect to vibrational, rotational, and spin-rotational motion of the neutral core.

In this paper, we focus on the autodetachment spectroscopy and dynamics of the vibrational ground state of the DBS and the spectroscopy of the ground electronic state of H_2CCC^- . The advantages of high resolution spectroscopy are fully utilized to observe spin-rotation splitting, asymmetry splitting, and to map out energy levels of the ground electronic states as well as the excited DBS. In addition, an interaction in the DBS between the $v'=0$ state and a vibrationally excited state is observed. Finally, we discuss the autodetachment lifetimes and attempt to elucidate the mechanisms of coupling between the electronic and nuclear degree of freedom operative in negative ions in general and H_2CCC^- in particular.

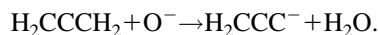
II. EXPERIMENT

A detailed description of the coaxial ion-beam spectrometer used in this experiment has been reported elsewhere.^{1(b)} Here we briefly outline ion formation, mass selection of the ions, the laser system, and data acquisition.

The $CCCH_2^-$ ions are produced by the reaction¹⁵ of allene with O^- . A 1:1 mixture of allene and N_2O gases at a pressure of 3 Torr passes through a 1 mm pinhole into a vacuum chamber at a pressure of 10^{-4} Torr. The gas flow is crossed with a 100 μA , 100 eV beam of electrons. The electron source consists of a coiled tungsten filament and a repeller plate.¹⁶ The O^- reactant is produced by dissociative attachment to N_2O . The desired H_2CCC^- is formed via the

^{a)}Present address: Department of Chemistry, Simon Fraser University, Burnaby, British Columbia, Canada, V5A 1S6.

H_2^+ abstraction reaction,



Negative ions formed in the source region are extracted and sent into a 90° magnetic mass sector where a mass-to-charge ratio of $m/e=38$ is selected. A typical H_2CCC^- ion current is ~ 2.5 nA. This mass selected ion beam is accelerated to 2.3 keV and bent another 90° by electrostatic bending quadrupoles where it enters the high vacuum ($\sim 10^{-9}$ Torr) interaction region. The ion beam is then merged coaxially with a counterpropagating laser beam. Therefore, the observed detachment energy is Doppler shifted ~ 5 cm^{-1} lower in frequency (but precisely determinable from the ion beam energy) than the actual transition energy. The initial energy spread of the ions in the source is kinematically compressed to 30 MHz, and is the dominant component in determining the experimental energy resolution. This effusive source produces ions of rather high temperature (estimated to be greater than 500 K). Usually a high temperature source is considered to be a disadvantage resulting in congested spectra. However, this high temperature source is both advantageous and necessary for this work. Because of the rather high electronic binding energy of the H_2CCC^- dipole-bound state (≈ 170 cm^{-1}), low J levels for $K'_a \leq 4$ are bound and thus are not detected. Therefore, significant population of rotational energy levels with $K''_a \geq 4$ in the ground electronic state must be present before we can observe the autodetachment resonances in the excited dipole-bound state.

As both C_3H_2 and its anion can exist in several isomeric forms, it was necessary to confirm formation of the negative ion of propadienylidene (H_2CCC^-) by photoelectron spectroscopy (PES).¹⁷ Further confirmation was obtained by isotopic substitutions. When D_2CCCH_2 was reacted with O^- , mass analysis showed only D_2CCC^- or H_2CCC^- as the major C_3 anionic products. Specifically, the formation of propargylene (HCCCD^-) was not observed.

The light source is a homebuilt ring dye laser using DCM dye pumped by an Ar^+ laser. This laser system can operate in two different configurations: one for low resolution survey scans and the other for high resolution scans. For survey scans the laser is used in a standing wave configuration with a resolution of 1 cm^{-1} and an average 800 mW of output power. For high resolution scans, the laser is used in the ring configuration with single mode operation (1 MHz linewidth) and an average 350 mW of output power. Scans are computer controlled with the starting and ending frequencies of each scan measured to ± 0.005 cm^{-1} by a lambda meter (traveling Michelson interferometer) utilizing a polarization stabilized He-Ne laser reference. The fringe patterns of a confocal Fabry-Perot etalon ($\text{FSR} \approx 250$ MHz) are collected simultaneously and are used to linearize the frequency scale of the data. High resolution data have been obtained from 14 000 to 15 000 cm^{-1} .

Low kinetic energy photodetached electrons ($< \sim 35$ meV) in the laser-ion interaction region of the spectrometer are captured inside a molybdenum tube surrounded by a solenoid magnet which provides a weak magnetic field (~ 2 G) along the beam axis. This produces cyclotron orbital motion

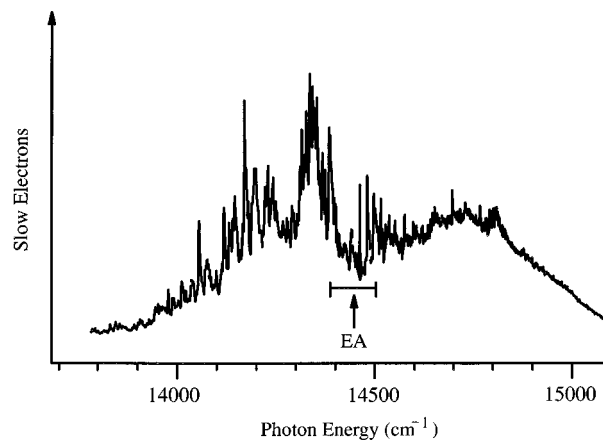


FIG. 1. Broadband scan of the threshold photodetachment region of H_2CCC^- (resolution ~ 1 cm^{-1}) detecting slow (~ 15 meV) electrons. The electron affinity (EA) obtained by negative ion photoelectron spectroscopy is shown with an error bar of ± 64 cm^{-1} .

of the electrons which in turn discriminates against higher kinetic energy electrons. These electrons are guided into a ceramic electron multiplier and detected as photodetachment signals. The electron counts are normalized to the ion beam current and the laser beam power and collected as a function of laser frequency. The range of linewidths (lifetimes) that can be measured is from 30 MHz (~ 5 ns) to 150 GHz (~ 1 ps). As mentioned earlier, the 30 MHz limit arises from the residual Doppler width from the initial velocity spread of ions in the source region. The upper limit is an empirical value which we are able to observe from the spectra.

III. OBSERVED SPECTRA

In the present experiment, a survey scan of detachment signal was carried out with 1 cm^{-1} resolution. The electron affinity (EA) of H_2CCC was determined¹⁷ by negative ion photoelectron spectroscopy to be 1.794 ± 0.008 eV, i.e., $14\,469 \pm 64$ cm^{-1} . We show the broadband scan of the threshold electron spectrum in Fig. 1 over a 1000 cm^{-1} range in the vicinity of the EA.

Two processes are at work in this photon energy region. The first is direct photodetachment from populated vibrational-rotational levels of the negative ion ground electronic state to a number of (neutral+electron) continuum states. This is a bound-free process and the ~ 500 K ion temperature gives rise to a large number of unresolved rovibronic thresholds. Since the measurement technique discriminates against fast electrons, the direct detachment signal drops off at energies well above threshold, as is observed in the region of $14\,800$ cm^{-1} in Fig. 1.

The second process involves a transition from rovibrational levels of the ground electronic state to quasibound levels of an excited, dipole-bound state (DBS) of the anion which subsequently undergoes autodetachment. These bound-quasibound processes produce strong resonances in the photodetachment spectrum which completely dominate the bound-free transitions throughout the region shown in Fig. 1. The low resolution spectrum exhibits strong autode-

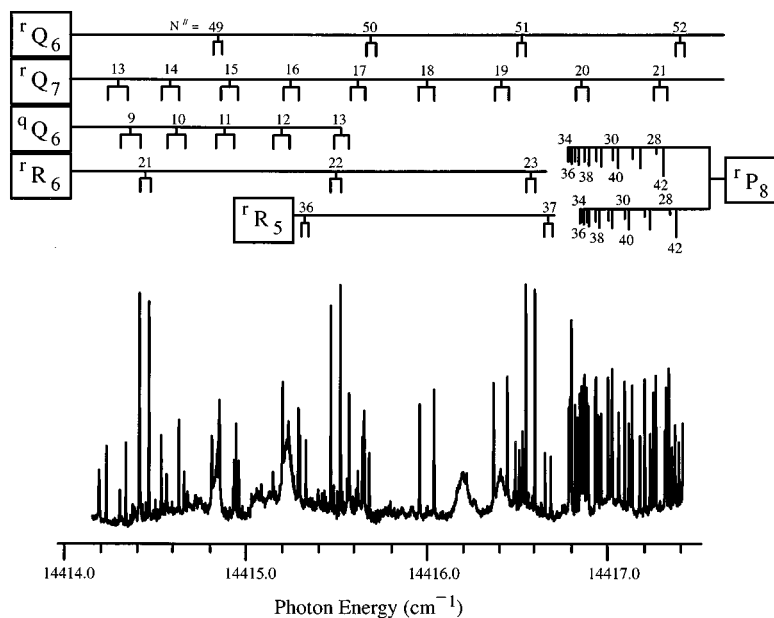


FIG. 2. High resolution ($300\times$) expansion of a selected portion of the spectrum in Fig. 1. The rotational assignments are shown in the portion. (See text for labeling.) The lines originate primarily from 0_0^0 transitions, and only the band labeled qQ_6 arises from 6_0^1 . The spin-rotation splitting of each progression is marked under the rotational number assignment.

tachment resonances both above and below the EA. In addition to the transition between vibrationless levels occurring near the EA, there are substantial contributions to the spectrum from populated excited vibrational levels, especially the CCC out-of-plane and in-plane bending modes. A detailed description of the structure and dynamics of these vibrationally excited states is given in the accompanying paper.¹⁸ In this paper, we focus on vibrational ground states for both the electronic ground state and the DBS.

The H_2CCC^- ion is a near-prolate symmetric top. The 0_0^0 band gives a type (c) transition with selection rules $\Delta K_a = \pm 1$ and $\Delta K_c = 0, \pm 2$. A total of 2538 transitions were assigned to the 0_0^0 band. Rotational levels belonging to K'_a between 0 and 4 of the DBS were not observed, because these levels either were stable or, if quasibound, did not autodetach within our experimental time window. Therefore, analysis of the 0_0^0 band could not provide information about rotational levels of $K_a \leq 4$ for the excited state (DBS) nor those of $K_a < 4$ for the ground state. Another band system was analyzed to obtain information on the lower state K_a levels of the anion ground state. Since the 6_0^1 band accesses energy levels above the binding energy, this band was utilized to obtain the ground state energy levels from $K''_a = 0$ to 3.

A high resolution scan with a resolution of 0.001 cm^{-1} was carried out in the region from $14\,000$ to $15\,000 \text{ cm}^{-1}$. A very small portion of this spectrum shown in Fig. 2 reveals the existence of many pairs of lines which have a splitting of $\sim 0.1 \text{ cm}^{-1}$. The electronic spin multiplicities of the ground and dipole-bound states of H_2CCC^- are doublet states. Therefore, the observed transitions are doublet-doublet transitions and spin-rotation splitting is clearly observed. In the present work, several bands frequently overlap, making the

assignment of each line difficult and possibly uncertain. However, there are some important features that make the assignment simpler and ensure correctness.

Since H_2CCC has C_{2v} symmetry, the nuclear spin statistics are similar to H_2O , i.e., the asymmetric and symmetric levels have statistical weights of 3:1 for symmetric vibronic states.¹⁹ For H_2CCC^- , the ground electronic state has 2B_1 character. Thus, the statistical weights for the even and odd K_a levels are in the ratio of 3:1. The resulting intensity alternation greatly facilitates spectral identification. Also, the linewidths are vastly different depending on whether the electron is detached from the vibrational ground state or excited states. By using the above features, the set of P , Q , and R branches were assigned and combination differences were then used to confirm the assignments.

A diagram of representative transitions is shown in Fig. 3. Here, each transition is labeled as follows. The superscripts p , q , and r indicate $\Delta K_a = -1, 0,$ and $+1$, respectively; the middle letter is the selection rule for N ($\Delta N = -1, 0,$ and $+1$), the subscript represents the starting K''_a , and the number in parentheses is the starting N'' .

IV. SPECTROSCOPIC ANALYSIS

Figure 4 depicts the radical H_2CCC and its principal axes. Since this molecule is a near-prolate symmetric top, it has two asymmetry levels with different total parities. We could not detect asymmetry splitting in the 0_0^0 band. However, the asymmetry splitting of $K''_a = 0-3$ was observed in the 6_0^1 band and then utilized to obtain the difference between the B'' and C'' rotational constants of the ground state (0_0). In addition, there are two spin sublevels, $F_1(J=N+1/2)$ and $F_2(J=N-1/2)$. To calculate the energy levels of an asym-

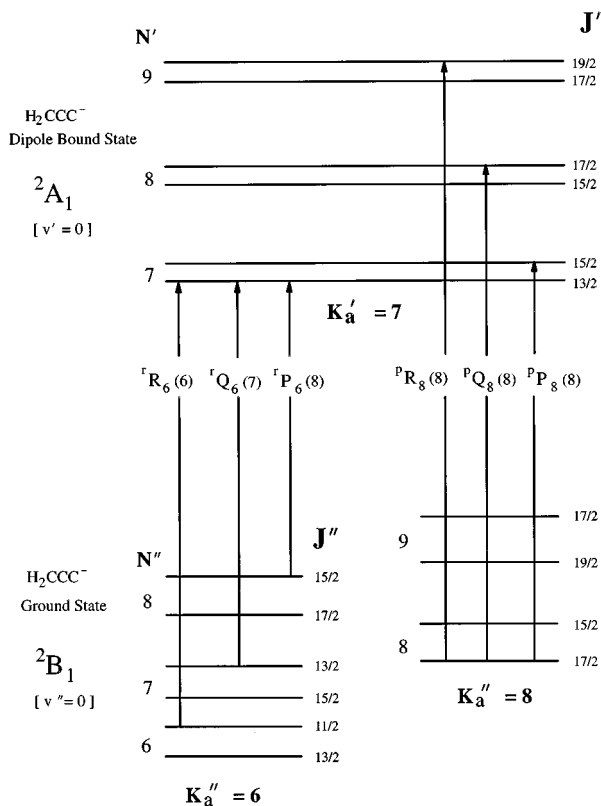


FIG. 3. Partial energy diagram for H₂CCC⁻. The excited electronic state has 2A_1 character and is best described as a dipole-bound state (DBS). Representative optical transitions are labeled. The spin-rotation splitting is exaggerated for clarity.

metric rotor, we start with a symmetric top basis set. The basis set used in this analysis is the Hund's case (b) basis functions given by $|N K S J M\rangle$, where N is the angular momentum of the nuclei, K is the angular momentum along the molecular figure axis, J is the total angular momentum about the space-fixed axis, M its projection onto the space-fixed axis, and S is the total electronic spin angular momentum. Then, we utilize the set of basis functions $|N K^\pm S J M\rangle$ by means of the Wang transformation²⁰

$$|N O^+ S J M\rangle = |N O S J M\rangle,$$

$$|N K^+ S J M\rangle = \frac{[|N K S J M\rangle + |N -K S J M\rangle]}{\sqrt{2}},$$

$$|N K^- S J M\rangle = \frac{[|N K S J M\rangle - |N -K S J M\rangle]}{\sqrt{2}}.$$

The model Hamiltonian, H used for analyzing this work, is Watson's S -reduced Hamiltonian,²¹ H_R with spin-rotation interaction, H_{SR} . That is,

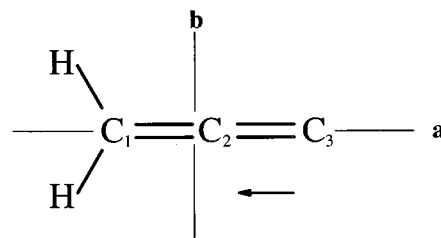


FIG. 4. Schematic of the structure of the radical H₂CCC⁻. The two internal axes and the direction of the dipole moment are shown with the hydrogens lying in the plane of the paper. The molecule-fixed c axis is perpendicular to the page. The equilibrium geometry is given by Ref. 30 as $r_e(C_1C_2)=1.3283\pm 0.0005$ Å, $r_e(C_2C_3)=1.291\pm 0.001$ Å, $r_e(C_1H)=1.083\pm 0.001$ Å, and $\angle(HC_1H)=117.6\pm 0.2^\circ$.

$$\begin{aligned} H &= H_R + H_{SR} \\ &= \left[A - \frac{B+C}{2} \right] \hat{N}_z^2 + \frac{B+C}{2} \hat{N}^2 - D_N \hat{N}^4 \\ &\quad - D_{NK} \hat{N}^2 \hat{N}_z^2 - D_K \hat{N}_z^4 + H_{NK} \hat{N}^4 \hat{N}_z^2 + H_{KN} \hat{N}^2 \hat{N}_z^4 \\ &\quad + H_K \hat{N}_z^6 - L_{NK} \hat{N}^4 \hat{N}_z^4 - L_{KN} \hat{N}^2 \hat{N}_z^6 + \left[\frac{B-C}{4} + d_1 \right] \\ &\quad \times (\hat{N}_+^2 + \hat{N}_-^2) + d_2 (\hat{N}_+^4 + \hat{N}_-^4) + H_{SR}, \end{aligned}$$

where $\hat{N}_\pm = \hat{N}_x \pm i\hat{N}_y$ and H_{SR} is the spin-rotation operator. The matrix elements of the H_R Hamiltonian are

$$\begin{aligned} \langle N K S J M | H_R | N K S J M \rangle &= \left(\frac{B+C}{2} \right) N(N+1) + \left[A - \frac{B+C}{2} \right] K^2 - D_N [N(N+1)]^2 \\ &\quad - D_{NK} N(N+1) K^2 - D_K K^4 + H_{NK} [N(N+1)]^2 K^2 \\ &\quad + H_{KN} N(N+1) K^4 + H_K K^6 \\ &\quad - L_{NK} [N(N+1)]^2 K^4 - L_{KN} N(N+1) K^6, \end{aligned}$$

$$\begin{aligned} \langle N K \pm 2 S J M | H_R | N K S J M \rangle &= \left[\frac{1}{4} (B-C) + d_1 N(N+1) \right] ([N(N+1) - K(K\pm 1)] \\ &\quad \times [N(N+1) - (K\pm 1)(K\pm 2)])^{1/2} \end{aligned}$$

and

$$\begin{aligned} \langle N K \pm 4 S J M | H_R | N K S J M \rangle &= d_2 [W X Y Z]^{1/2}, \end{aligned}$$

where

$$\begin{aligned} W &= [N(N+1) - K(K\pm 1)], \\ X &= [N(N+1) - (K\pm 1)(K\pm 2)], \\ Y &= [N(N+1) - (K\pm 2)(K\pm 3)], \end{aligned}$$

and

$$Z = [N(N+1) - (K\pm 3)(K\pm 4)].$$

The spin-rotation interaction Hamiltonian H_{SR} is expressed with use of rank k irreducible tensor $T^k(\epsilon)$ as²²

$$H_{\text{SR}} = \frac{1}{2} \sum_{k=0}^2 [\mathbf{T}^k(\boldsymbol{\epsilon}) \cdot \mathbf{T}^k(\hat{N}, \hat{S}) + \mathbf{T}^k(\hat{N}, \hat{S}) \cdot \mathbf{T}^k(\boldsymbol{\epsilon})],$$

where

$$T_p^k(\hat{N}, \hat{S}) = (-1)^p (2k+1)^{1/2} \sum_{p_1, p_2} T_{p_1}^1(\hat{N}) T_{p_2}^1(\hat{S}) \times \begin{pmatrix} 1 & 1 & k \\ p_1 & p_2 & -p \end{pmatrix}.$$

By transforming molecule-fixed components (q) to space fixed components (p),²³ we obtain

$$T_p^k(\boldsymbol{\epsilon}) = \sum_q D_{pq}^{k*}(\omega) T_q^k(\boldsymbol{\epsilon}).$$

The spin-rotation interaction matrix elements are expressed as

$$\begin{aligned} H_{\text{SR}} &= \langle N' K' S J' M' | H_{\text{SR}} | N K S J M \rangle \\ &= \delta_{MJ, M} \delta_{J', J} \sum_{k=0}^2 ((2k+1)S(S+1)(2S+1)(2N+1) \\ &\quad \times (2N'+1)^{1/2} (-1)^{J+S+N'} \begin{pmatrix} N & S & J \\ S & N' & 1 \end{pmatrix} \\ &\quad \times \frac{1}{2} \left[(-1)^k [N(N+1)(2N+1)]^{1/2} \begin{pmatrix} 1 & 1 & k \\ N' & N & N \end{pmatrix} \right. \\ &\quad \left. + [N'(N'+1)(2N'+1)]^{1/2} \begin{pmatrix} 1 & 1 & k \\ N & N' & N' \end{pmatrix} \right] \\ &\quad \times \sum_q (-1)^{N'-K'} \begin{pmatrix} N' & k & N \\ -K' & q & K \end{pmatrix} T_q^k(\boldsymbol{\epsilon}). \end{aligned}$$

In this analysis we retain only the dominant spin-rotation matrix elements, corresponding to $\Delta N=0$ or -1 ,²⁴

$$\begin{aligned} \langle N K S J M | H_{\text{SR}} | N K S J M \rangle \\ = -[\Gamma(NSJ)/2N(N+1)] [\epsilon_{aa} K^2 + \frac{1}{2} (\epsilon_{bb} + \epsilon_{cc}) \\ \times [N(N+1) - K^2]], \end{aligned}$$

$$\begin{aligned} \langle N-1 K S J M | H_{\text{SR}} | N K S J M \rangle \\ = -\phi(NSJ)(K/2N)(N^2 - K^2)^{1/2} [\epsilon_{aa} - \frac{1}{2} (\epsilon_{bb} + \epsilon_{cc})], \end{aligned}$$

where $\Gamma(NSJ) = N(N+1) + S(S+1) - J(J+1)$, $\phi(NSJ) = [(N-J+S)(N+J+S+1)(S+J-N+1)(N+J-S)/((2N+1)(2N-1))]^{1/2}$, and $\phi(NSJ)=1$ for $S=1/2$.

All observed lines were fitted to this model Hamiltonian, and best-fit parameters were derived by nonlinear least squares analysis. However, significant deviations from the model Hamiltonian were observed in the region of $K'_a = 7-10$. To visualize this phenomenon, the effective rotational constants of each K_a stack are plotted as a function of K_a^2 in Fig. 5. Note the large discontinuity in the rovibronic levels of the DBS between $K'_a = 7$ and $K'_a = 8$ as well as a deviation from the unperturbed value at $K'_a \geq 8$ of the 0^0 level. This interaction has been attributed to a centrifugal

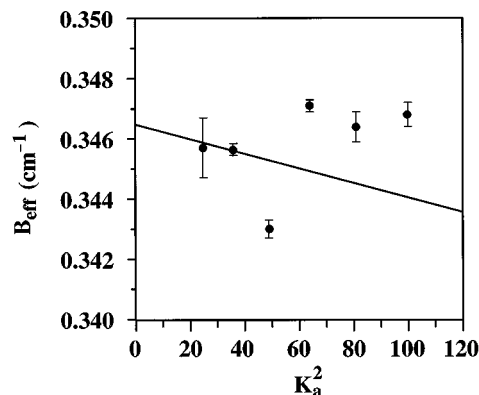


FIG. 5. Dependence of the effective rotational constants B_{eff} on K_a^2 for the 0^0 level of the DBS; the solid line is the deperturbed result.

distortion coupling²⁵ between $v'=0$ and 6^1 and between $v'=0$ and 9^1 of the dipole-bound state with specific K_a selection rules, i.e., $\Delta K_a = \pm 1$. A detailed analysis of this interaction is described elsewhere.²⁶

A. Molecular structure

The molecular constants are determined for the DBS and the electronic ground states using the Hamiltonian described by Eqs. (2) and (4) together with a nonlinear least squares fitting procedure. Since in the DBS, the 0^0 level interacts with the 6^1 and 9^1 levels as described above, the interaction has to be included when the eigenstates of the 0^0 level are obtained. However, we also observe strong Coriolis mixing between ν_6 and ν_9 modes in both ground electronic state and the DBS. A complete description of this interaction appears in the accompanying paper.¹⁸ This coupling must also be included in the fitting procedure. For this reason, the $0_0^0, 6_0^1, 6_1^1, 9_1^0$, and $6_0^1 9_1^0$ bands were fitted simultaneously to obtain the final molecular constants. The standard deviation of the total fit for the nearly 9000 transitions is $\sigma = 7.7 \times 10^{-3} \text{ cm}^{-1}$. The derived molecular constants of 0_0^0 are listed in Table I, along with those of H_2CCC neutral obtained by Virtilek *et al.*²⁷

From these anion excited state molecular constants, it is clear that the excited state has a geometry very similar to the neutral, as would be characteristic of a DBS. The molecular A , B , and C constants of the DBS match those of the neutral to within 0.2%. Further evidence of the DBS character comes from the observation that the spin-rotation interaction constant ϵ_{aa} of the excited state is one order of magnitude smaller than that of the ground electronic states of the anion. The known spin-rotation constant of isoelectronic H_2CCN is $\epsilon_{aa}(\text{H}_2\text{CCN}) = -2.19(2) \times 10^{-2} \text{ cm}^{-1}$,²⁸ comparable to the spin-rotation constant of H_2CCC^- in the vibrationless electronic ground state, found to be $\epsilon_{aa}''(\text{H}_2\text{CCC}^-) = -2.49(1) \times 10^{-2} \text{ cm}^{-1}$. Similarly, one would expect the spin-rotation coupling constant for a valence state of H_2CCC^- to be on the order of 10^{-2} cm^{-1} . However, in a DBS, the electron resides far from the neutral core and thus, interacts weakly with the rotation of the molecular core. As a result, the spin-multiplet splittings in the DBS are very small in comparison to those

TABLE I. Molecular constants of H₂CCC⁻ and ¹A₁ H₂CCC. All values in units of cm⁻¹.^a The total standard deviation (σ) is 7.7×10^{-3} cm⁻¹. Some 8700 transitions are fit, of which 2538 belong to the 0-0 transition. See text for details.

	² B ₁ H ₂ CCC ⁻ Ground state	² A ₁ H ₂ CCC ⁻ DBS ^b	¹ A ₁ H ₂ CCC Neutral ²⁷
<i>A</i>	9.731 48(4)	9.651 53(4)	<i>A</i> 9.632 76(114)
<i>B</i>	0.343 72(1)	0.346 461(3) ^c	<i>B</i> 0.353 19897(7)
<i>C</i>	0.331 51(1)		<i>C</i> 0.340 36766(7)
<i>D_N</i>	$9.7(1) \times 10^{-8}$	$5.5(1) \times 10^{-8}$	<i>D_J</i> $1.416 9(7) \times 10^{-7}$
<i>D_{NK}</i>	$1.04(1) \times 10^{-5}$	$2.42(1) \times 10^{-5}$	<i>D_{JK}</i> $1.7225(17) \times 10^{-5}$
<i>D_K</i>	$7.37(1) \times 10^{-4}$	$8.72(1) \times 10^{-4}$	<i>D_K</i> ^d 7.8504×10^{-4}
<i>d₁</i>	$-4.8(7) \times 10^{-8}$		<i>d₁</i> $-5.10(7) \times 10^{-9}$
<i>d₂</i>	$5(1) \times 10^{-9}$		<i>d₂</i> $-2.33(3) \times 10^{-9}$
<i>H_{NK}</i>	$-2.34(6) \times 10^{-9}$	$-1.56(5) \times 10^{-9}$	<i>H_{JK}</i> $2.53(8) \times 10^{-10}$
<i>H_{KN}</i>	$-1.81(3) \times 10^{-7}$	$1.45(3) \times 10^{-7}$	<i>H_{KJ}</i> $-4.26(24) \times 10^{-8}$
<i>H_K</i>	$-2.7(1) \times 10^{-7}$	$-8.36(8) \times 10^{-7}$	
<i>L_{NK}</i>	$-5.58(8) \times 10^{-11}$	$-3.58(5) \times 10^{-11}$	
<i>L_{KN}</i>	$9.8(3) \times 10^{-10}$	$3.2(1) \times 10^{-10}$	<i>L_{KJ}</i> $2.0(1) \times 10^{-9}$
ϵ_{aa}	$-2.49(1) \times 10^{-2}$	$2.17(6) \times 10^{-3}$	
$[\epsilon_{bb} + \epsilon_{cc}]/2$	$1.70(1) \times 10^{-3}$	$1.271(5) \times 10^{-3}$	
ν_0		14 284.420(5)	
σ	0.0077		
Δ	0.074(3)		0.0493(2)

^aThe molecular constants of X ¹A₁ H₂CCC are shown for comparison. The anion ²A₁ DBS was perturbed by the vibrationally excited state. Therefore, the upper level was deperturbed and the deperturbed molecular constants are reported here. The quantity Δ is the inertial defect (amu \AA^2).

^bThe centrifugal distortion coupling terms were also included in order to reproduce the energy level of this state. The centrifugal distortion constants are $C_6^{ac} = 1.0723(2) \times 10^{-4}$ and $C_9^{ab} = -1.5397(5) \times 10^{-5}$, respectively (Ref. 30).

^cThe value of $[B + C]/2$ is given here. The corresponding value for the neutral is 0.346 783 28(7) cm⁻¹.

^dConstrained to the *D_K* value for ketene because of high correlation with *A*.

of the anion ground state. The absolute value of spin-rotation constant ϵ_{aa} obtained for the DBS is smaller than that for the ground electronic state by approximately a factor of 10, $\epsilon'_{aa}(\text{DBS}) = 2.17(6) \times 10^{-3}$ cm⁻¹.

Because we have not investigated the isotopic variants, only limited structural information can be extracted from the rotational constants. It is, however, possible to obtain structural information by constraining some structural parameters during the fitting procedure. First, the planarity of the molecule can be determined from the inertial defect, $\Delta = I_c - I_a - I_b$. If $\Delta \geq 0$, the molecule has a planar structure,²⁹ while a negative Δ suggests a nonplanar structure. As shown in Table I, the ground state of H₂CCC⁻ has $\Delta = 0.074(3)$ amu \AA^2 and is planar.

Asymmetry splitting was not observed for the DBS, so precise *B* and *C* rotational constants could not be obtained and the issue of DBS planarity could not be addressed by our data. Since the structure of the DBS is quite similar to that of the neutral, however, it is plausible to assume that the DBS is also planar. We can then derive the H–C₁–H angles by using the rotational *A* constants in Table I and assuming that the C₁–H bond lengths are the same in all of these species. On this basis, the H–C₁–H bond angle for the DBS is calculated to be 118.5(2)° and the H–C₁–H angle for the ground state negative ion is 117.7(2)°. The H–C₁–H bond angle for the neutral had been determined as 117.6 ± 0.2°.³⁰

B. Binding energy

The binding energy of the dipole bound electron in the excited state of H₂CCC⁻ can be approximated as follows. From the measured band origin [14 284.420(5) cm⁻¹] and the electron affinity (14 469 ± 64 cm⁻¹), as measured by PES,¹⁸ we obtain the binding energy E_{bind} to be 14 469 ± 64 – 14 284.420(5) = 185 ± 64 cm⁻¹, i.e., 121 cm⁻¹ ≤ E_{bind} ≤ 249 cm⁻¹. If one can observe any levels of the DBS that lie below 15 533 cm⁻¹ (14 469 + 64 cm⁻¹), this observation would further refine the upper bound. We have observed autodetachment from the lowest rotational level (i.e., $K'_a = 0$, $N' = 0$, and $J' = 0.5$) of the vibrational band $\nu'_6 = 1$, which has an energy of 221.5 cm⁻¹ above the reported EA (corresponding to 14 505 cm⁻¹). This places an upper limit on E_{bind} ($E_{\text{bind}} \leq 221$ cm⁻¹) and thus the binding energy can be further refined to be 170 ± 50 cm⁻¹.

Suppose that the only force binding the outer electron is due to the dipole moment-charge interaction given by a point dipole potential, $U(r, \theta)$. The radial dipole force $F_{\text{dip}}(r, \theta)$ is then given as

$$F_{\text{dip}} = -\frac{\partial U}{\partial r} = -\frac{\partial(eD \cos \theta / 4\pi\epsilon_0 r^2)}{\partial r} = \frac{2eD \cos \theta}{4\pi\epsilon_0 r^3},$$

where e is the electron charge in Coulombs, μ is the dipole moment in debye, r is the electron distance from the dipole,

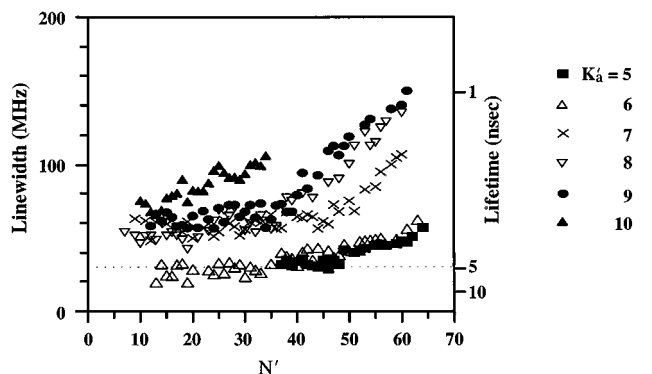


FIG. 6. Autodetachment rates (lifetimes) of H_2CCC^- $v'=0$ level of the DBS as a function of DBS rotational quantum number N' for various K'_a sublevels. The dotted line shows the 30 MHz instrument limit of the apparatus.

and θ is the angle between the dipolar axis and the electron's position. The binding energy of the dipole bound state can therefore be approximated as

$$E_{\text{bind}} = \frac{e\mu}{4\pi\epsilon_0 r_{\text{dip}}^2}.$$

Upon substituting a binding energy of 170 cm^{-1} and dipole moment of 4.5 D ,¹⁸ the most probable radius of the outer electron r_{dip} is found to be $\sim 25\text{ \AA}$.

V. AUTODETACHMENT DYNAMICS

A. Autodetachment lifetimes

The observed sharp features arise from resolved quasi-bound autodetaching states within the DBS manifold and therefore each feature can be associated with an autodetachment rate. In our apparatus, the ion beam remains in the interaction region for $\sim 3\text{ }\mu\text{s}$. Thus, states that have lifetimes longer than $3\text{ }\mu\text{s}$ will be inefficiently detected. The instrumental resolution limit, determined by Doppler kinematic compression of the ion beam, is approximately 30 MHz. Only linewidths greater than 30 MHz are studied to measure the autodetachment rates; those possessing smaller intrinsic linewidths would appear with a 30 MHz linewidth, but with reduced intensity owing to the slow autodetachment.

The observed electron signal arises from both direct photodetachment and a bound-bound transition followed by autodetachment. This phenomenon is similar to autoionization or predissociation processes that exhibit asymmetric line broadening due to an interference effect during a transition from a lower state to an upper bound-continuum mixed state. The absorption cross section of an individual resonance has a shape described by a Fano profile.³¹ In the present case, the autodetachment cross section was typically 100 times larger than the direct photodetachment. In this weak coupling limit, the Fano asymmetry parameter is very small, and the autodetachment resonances become symmetric, giving a Lorentzian line shape. All observed lines exhibited profiles that could be fit with a Lorentzian line shape.

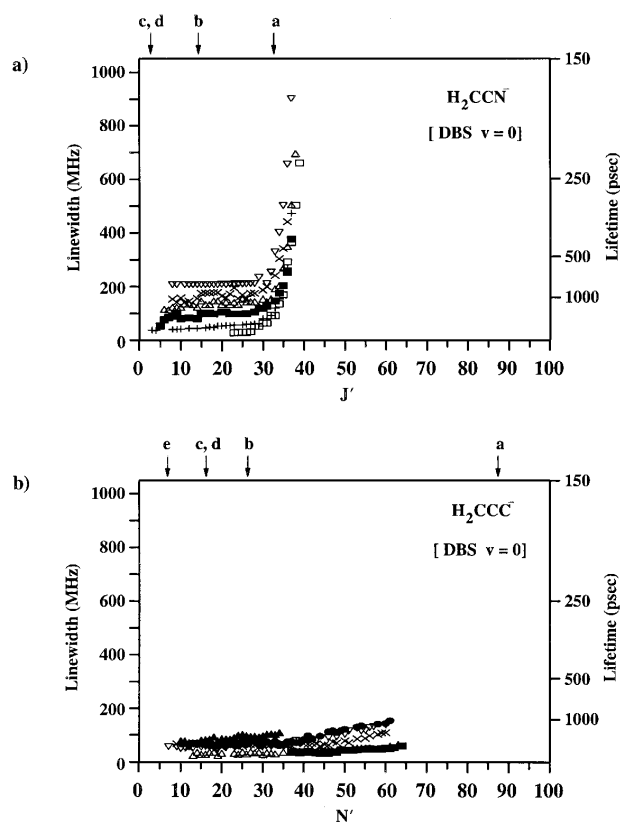


FIG. 7. Autodetachment lifetime as a function of the upper rotational quantum number. Two plots, (a) H_2CCN^- (reproduced from Ref. 3) and (b) H_2CCC^- (this work) are shown on the same scale. The quantum number N' (H_2CCC^-) or $J(\text{H}_2\text{CCN}^-)$ at which autodetachment channels become energetically allowed is indicated by the arrows a, b, c, d, and e. These detachment channels are characterized by: a, $\Delta K'_a=0$, $\Delta N(J)\leq 3$; b, $\Delta K'_a=0$, $\Delta N(J)\geq 4$; c, $\Delta K'_a=2$, $\Delta N(J)=2$; d, $\Delta K'_a=2$, $\Delta N(J)\geq 3$; and e, $\Delta K'_a=4$, $\Delta N(J)\leq 3$. The rapid increase in the H_2CCN^- autodetachment rate is associated with the opening of the channel labeled a. The corresponding channel in H_2CCC^- does not open until $N'\approx 90$, and could not be observed. (a) H_2CCN^- , \square , $K'_a=1$; $+$, $K'_a=3$; \blacksquare , $K'_a=5$; \triangle , $K'_a=6$; \times , $K'_a=7$; ∇ , $K'_a=8$; (b) H_2CCC^- , \blacksquare , $K'_a=5$; \triangle , $K'_a=6$; \times , $K'_a=7$; ∇ , $K'_a=8$; \bullet , $K'_a=9$; \blacktriangle , $K'_a=10$.

Fits were optimized by visual inspection and the resulting FWHM was extracted from the fit. The observed autodetachment rates are shown in Fig. 6 for $K'_a=5$ to 10 as a function of rotational quantum number N' of the excited state. There is a slight linewidth dependence on rotational level (N') between different K'_a stacks. Both $F1$ and $F2$ spin sublevels display the same FWHM within the experimental error.

B. Comparison of autodetachment rates of H_2CCC^- and H_2CCN^- (D_2CCN^-)

The molecular structures of H_2CCC^- and H_2CCN^- (D_2CCN^-) are quite similar. Differences in their autodetachment rates arise primarily from the consequences of replacing a nitrogen atom in H_2CCN^- with a carbon atom in H_2CCC^- . This results in a 21% increase (from 3.7 debye ³² to 4.5 debye ¹⁸) in the dipole moment of the neutral core and represents a substantial difference in electronic structure.

The autodetachment dynamics of H₂CCC⁻ differs from that observed for H₂CCN⁻ in that the dramatic dependence of the H₂CCN⁻ autodetachment rate on rotational level³ does not occur for H₂CCC⁻. In order to clarify this, the autodetachment rate as a function of upper rotational level for H₂CCN⁻ is compared to that of H₂CCC⁻ in Fig. 7(a) and (b). The autodetachment rate up to $J'(N')=30$ is quite similar both qualitatively and quantitatively. However, there is a rapid increase in the rotational detachment rate of H₂CCN⁻ at $J' \approx 33$; no such behavior is found for H₂CCC⁻. This difference is largely a consequence of the greater dipole moment (and binding energy) in H₂CCC⁻.

C. Autodetachment mechanism

The detailed mechanism of autodetachment from dipole-bound states has been well described in previous studies.^{1-5,32,33} Here we summarize some aspects that are necessary to an understanding of the autodetachment dynamics. Autodetachment arises from a breakdown of the Born–Oppenheimer approximation, in which the quasibound states couple with the continuum states and rotational, vibrational, or electronic energy is utilized in the electron detachment process. The detachment rates are well described by the Fermi Golden Rule

$$\text{Rate} \propto \frac{2\pi}{\hbar} |\langle \psi_f | \hat{T} | \psi_i \rangle|^2 \rho,$$

where \hat{T} is the coupling operator, Ψ_f is the final state wave function, Ψ_i is the initial state wave function, and ρ is the density of final states. There are four coupling operators that can give rise to autodetachment: (1) configuration interaction (electron–electron coupling), (2) spin-orbit coupling, (3) vibrational–electronic coupling, and (4) rotational–electronic coupling. In the study of autodetachment dynamics carried out previously on the vibrationless levels of H₂CCN⁻,³ rotational–electronic coupling was found to be the dominant autodetachment mechanism.

For the H₂CCC⁻ DBS, however, certain regions of the ground vibrational state are strongly coupled to the vibrationally excited 6¹ and 9¹ states. Our results indicate that there is little or no contribution from vibrational–electronic coupling anywhere, even in the perturbed regions. The autodetachment rate from the 6¹ state was measured to be 2 to 3 times faster than corresponding levels of the 0⁰ state.¹⁸ If vibrational–electronic coupling were important, then one would have expected to observe an increase in linewidth of the perturbed levels.

As for H₂CCN⁻, rotational–electronic coupling is the main mechanism considered in this study. Since the DBS structure is very similar to that of the neutral, we employ the formalism for Rydberg state autoionization introduced by Berry.³⁴ In this model, the interaction term associated with rotational–electronic coupling is written as

$$\hat{T} \propto -\frac{\hbar^2}{2\mu R^2} \hat{N}_{\text{el}} \cdot \hat{N}_{\text{rot}},$$

where \hat{N} indicates the rotational angular momentum operator (\hat{N}_{el} operates on the electronic wave function, and \hat{N}_{rot} on the rotational wave function), μ is the reduced mass, and R is a relevant nuclear distance.

The stability of the DBS orbital can be described as a function of the type of rotational motion. Since the DBS diffuse electronic orbital resides on the positive side of the neutral dipole core, the molecular a axis passes directly through this orbital, and rotation about the molecule fixed a axis does not disturb it significantly; in contrast, the end-over-end rotational (b or c axis) motion perturbs the DBS orbital quite dramatically. These trends were quite pronounced in the case of H₂CCN⁻ and D₂CCN⁻, where autodetachment rates were significantly enhanced at levels higher than $J' \approx 33$ and $J' \approx 38$ in the case of H₂CCN⁻ and D₂CCN⁻,³ respectively. However, autodetachment of H₂CCC⁻ differs in that there is a slight increase in the autodetachment rate as N' increases, but no sharp onset as seen in H₂CCN⁻. The main difference between the two molecular systems is the size of the dipole moment of the neutral core, that is, the field strength that binds the outer electron. The DBS of H₂CCC⁻ has a larger binding energy ($E_{\text{bind}} \approx 170 \text{ cm}^{-1}$) than that of H₂CCN⁻ ($E_{\text{bind}} \leq 66 \text{ cm}^{-1}$). This shifts the entire DBS rotational energy manifold of H₂CCC⁻ lower with respect to the neutral rotational levels by approximately 105 cm^{-1} , relative to the case of H₂CCN⁻. The sharp increase seen at $J \approx 33$ would likely appear at $N \approx 90$ for H₂CCC⁻.

The propensity rule for changes in K_a as a result of rotational autodetachment can be understood as follows. Since the nuclear spin should be unchanged before and after autodetachment, the sign of the nuclear spin wave function must be invariant. Thus, K_a has to change by an even number, $\Delta K_a = 0, \pm 2, \pm 4, \dots$. Autodetachment will be favored for the processes that involve the smallest change in first the rotational quantum numbers K_a and second the rotational quantum number $N(J)$. A large mismatch in energy between the DBS and neutral state energy levels will lead to a large difference in angular momentum between the DBS and the neutrals, creating a substantial centrifugal barrier for the departing electron. The difference in angular momentum (l) between the DBS and the neutrals must be carried by the outgoing electron, creating a centrifugal barrier given by

$$E_{\text{barrier}} = \frac{\hbar^2 l(l+1)}{2m_e r^2},$$

where r is the distance of the electron from the center of mass and m_e is the mass of the electron.

An increase in the autodetachment rate corresponds to the opening of additional detachment channels as can be clearly seen in the case of H₂CCN⁻. The observed onset in H₂CCN⁻ is ascribed to opening of the detachment channel satisfying $\Delta K_a = 0$, $\Delta N(J) \geq 3$, labeled “a” in Fig. 7(a). The other (weaker) detachment channels labeled as b, c, and d correspond to $\Delta K_a = 0$, $\Delta N(J) \geq 4$, $\Delta K_a = 2$, $\Delta N(J) = 2$, and $\Delta K_a = 2$, $\Delta N(J) \geq 3$, respectively.

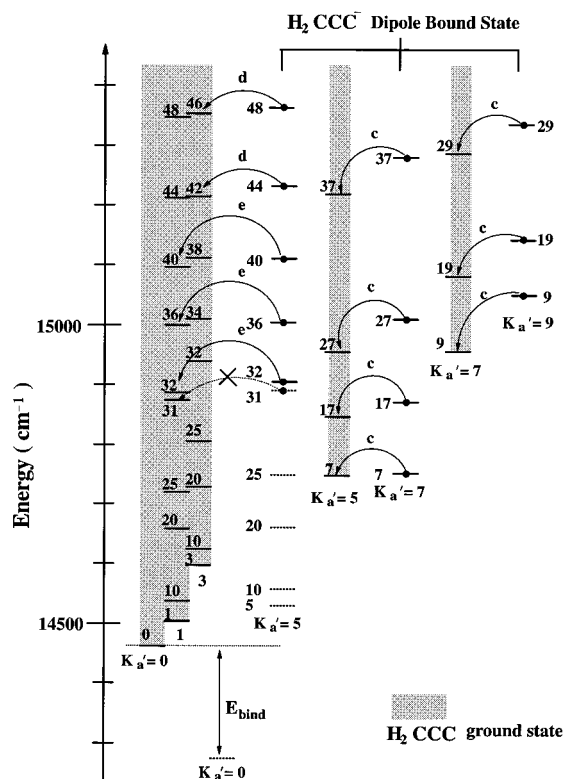


FIG. 8. A portion of the energy level diagram of the H_2CCC^- DBS and H_2CCC neutral is shown to illustrate several different rotational autodetachment channels. The levels of the neutral are overlaid with shaded rectangles. The figure is shown for a 195 cm^{-1} DBS binding energy and an $14\,469\text{ cm}^{-1}$ EA. The detachment channels indicated by letters c, d, and e correspond to the detachment channels labeled in Fig. 7. X indicates that autodetachment was not observed for levels with $K'_a = 5$ and $N' < 32$ because of the centrifugal barrier.

In addition to the above four detachment channels, one other detachment channel is required to explain the observed detachment dynamics in H_2CCC^- . We observe that autodetachment from $K'_a = 5$ is only about 15% as strong as that for $K'_a \in [H^<]_{\text{xxx}} \geq 6$ by measuring the integrated intensity of each rotational line. The result strongly suggests that the opening detachment channel for the range of N reported here must be $\Delta K_a = 4$. This would be the case if E_{bind} were 195 cm^{-1} , shown schematically in Fig. 8. This in turn sets a constraint on the DBS binding energy. The lowest observed rotational level of $K'_a = 5$ was $N' = 32$, approximately 400 cm^{-1} above the binding energy. The reason we did not see detachment from the rotational levels above the binding energy up to the level of $K'_a = 5, N' = 32$ can be explained by the centrifugal barrier. This barrier must also be a function of K_a since one can see detachment from $K'_a = 7$ to $K'_a = 5$ of the neutral. The detachment channel labeled “a” results in a significant enhancement in autodetachment rate in H_2CCN^- but remains closed for H_2CCC^- until $J'(N') \approx 90$ as indicated in Fig. 7(b).

To understand the autodetachment dynamics of H_2CCN^- from a theoretical point of view, Clary³² has calculated rotationally adiabatic potentials for the dipole-bound states and predicted the expected linewidths. This model has

been further modified by Simons³³ to predict the autodetachment rate enhancements seen for $N(J) > 30$ and to treat the branching ratios for the formation of neutrals in various rotational states. These models can be applied to the case of H_2CCC^- , and successfully predict the rapid increase in the autodetachment rate when the $\Delta K_a = 0$, $\Delta N(J) \leq 3$ channel becomes accessible. However, a combination of the angular momentum barrier and the anisotropic dipole potential makes for complicated trajectories for the outgoing electron. The electron is localized on the positive end of H_2CCC until it becomes decoupled. The electron does not experience the angular momentum barrier until it begins to decouple from the internuclear axis and acquires orbital angular momentum. A solution of this problem would require a quantum mechanical frame transformation.³⁵

We note that multichannel quantum defect theory (MQDT) in conjunction with the frame transformation technique was successfully used to treat autodetachment of H^- by Sadeghpour and Greene.³⁶ The rotational and vibrational autoionization of Rydberg electrons in a polyatomic molecule case has also been recently treated for H_3^+ , including the Jahn–Teller interaction.³⁷ Autodetachment rates relevant to the present case should, in principle, be calculated accurately by the MQDT frame transformation method, but this calculation is nontrivial for polyatomic molecules with five atoms.

VI. CONCLUSIONS

Autodetachment spectroscopy with a coaxial laser-ion beam spectrometer provides a sensitive means to obtain detailed information about both the ground state and weakly bound electronically excited states of negative ions. In the case of H_2CCC^- , term energies and linewidth measurements have yielded substantial information about the properties of dipole-bound states in terms of both structure and rotational-electronic coupling autodetachment dynamics. The present study with rotational resolution provides considerable insight into the intramolecular interaction taking place between vibrationally excited and ground states of the DBS. Autodetachment dynamics of H_2CCC^- has been compared to the structurally similar H_2CCN^- . The autodetachment rates of the two systems showed a qualitatively and quantitatively similar dependence on rotational motion up to $N(J) \leq 33$. The major difference was seen at $N(J) \geq 33$, where H_2CCN^- exhibits a rapid increase in the rotational autodetachment rates whereas H_2CCC^- shows no significant enhancement. This difference is attributed to the significant increase in binding energy for H_2CCC^- between the DBS and the neutral, and the concomitant increase in the centrifugal barrier seen by the autodetaching electron. The observed autodetachment rates of H_2CCC^- suggest the binding energy of the DBS to be $\sim 195\text{ cm}^{-1}$. The detachment channel corresponding to the significant onset of rotational autodetachment is $\Delta K_a = 0$, $\Delta N(J) \leq 3$, and is estimated to be closed for H_2CCC^- up to energies where $N \approx 90$.

ACKNOWLEDGMENTS

The authors are grateful for experimental help in the early stages from A. S. Mullin and D. M. Szaflarski. We would also like to thank J. A. Stephens and P. J. Campagnola for stimulating discussions. G.W.L. wishes to thank the Natural Sciences and Engineering Research Council of Canada for support under an NSERC postdoctoral fellowship. The financial support of National Science Foundation, Grant Nos. PHY95-12150 and CHE93-8639, and the Air Force Office of Scientific Research is gratefully acknowledged.

- ¹(a) K. R. Lykke, R. D. Mead, and W. C. Lineberger, *Phys. Rev. Lett.* **52**, 2221 (1984); (b) R. D. Mead, K. R. Lykke, W. C. Lineberger, J. Marks, and J. I. Brauman, *J. Chem. Phys.* **81**, 4883 (1984); (c) A. S. Mullin, K. K. Murray, C. P. Schultz, D. M. Szaflarski, and W. C. Lineberger, *Chem. Phys.* **166**, 207 (1992).
- ²T. Andersen, K. R. Lykke, D. M. Neumark, and W. C. Lineberger, *J. Chem. Phys.* **86**, 1858 (1987).
- ³K. R. Lykke, D. M. Neumark, T. Andersen, V. J. Trapa, and W. C. Lineberger, *J. Chem. Phys.* **87**, 6842 (1987).
- ⁴J. Marks, J. I. Brauman, R. D. Mead, K. R. Lykke, and W. C. Lineberger, *J. Chem. Phys.* **88**, 6785 (1988).
- ⁵A. S. Mullin, K. K. Murray, C. P. Schultz, and W. C. Lineberger, *J. Phys. Chem.* **97**, 10281 (1993).
- ⁶A. H. Zimmerman and J. I. Brauman, *J. Chem. Phys.* **66**, 5823 (1977); R. L. Jackson, A. H. Zimmerman, and J. I. Brauman, *ibid.* **71**, 2088 (1979).
- ⁷R. L. Jackson, P. C. Hiberty, and J. I. Brauman, *J. Chem. Phys.* **74**, 3705 (1981).
- ⁸J. Marks, P. B. Comita, and J. I. Brauman, *J. Am. Chem. Soc.* **107**, 3718 (1985).
- ⁹E. A. Brinkman, S. Berger, J. Marks, and J. I. Brauman, *J. Chem. Phys.* **99**, 7586 (1993).
- ¹⁰J. A. Stockdale, F. J. Davis, R. N. Compton, and C. E. Klots, *J. Chem. Phys.* **60**, 4279 (1974).
- ¹¹C. E. Klots, *J. Chem. Phys.* **62**, 741 (1975).
- ¹²C. Desfrancois, H. Abdoul-Carime, C. Adjouri, N. Khelifa, and J. P. Schermann, *Europhys. Lett.* **26**, 25 (1994).
- ¹³R. A. Popple, C. D. Finch, and F. B. Dunning, *Chem. Phys. Lett.* **234**, 172 (1995).
- ¹⁴S. M. Trujillo, R. H. Neynaber, and E. W. Rothe, *Rev. Sci. Instrum.* **37**, 1655 (1966).
- ¹⁵J. H. J. Dawson and K. R. Jennings, *J. Chem. Soc. Faraday II* **72**, 700 (1976); J. Lee and J. J. Grabowski, *Chem. Rev.* **92**, 1611 (1992).
- ¹⁶A. S. Mullin, D. M. Szaflarski, K. Yokoyama, G. Gerber, and W. C. Lineberger, *J. Chem. Phys.* **96**, 3636 (1992).
- ¹⁷M. S. Robinson, M. L. Polak, V. M. Bierbaum, C. H. DePuy, and W. C. Lineberger, *J. Am. Chem. Soc.* **117**, 6766 (1995).
- ¹⁸K. Yokoyama, G. W. Leach, J. B. Kim, W. C. Lineberger, A. I. Boldyrev, and M. Gutowski, *J. Chem. Phys.* **105**, 10706 (1996).
- ¹⁹G. Herzberg, *Electronic Spectra of Polyatomic Molecules* (Van Nostrand, New York, 1967).
- ²⁰S. C. Wang, *Phys. Rev.* **34**, 243 (1929).
- ²¹J. K. G. Watson, in *Vibrational Spectra and Structure*, edited by J. R. Durig (Elsevier, Amsterdam, 1977), Vol. 6, p. 1.
- ²²A. R. Edmonds, *Angular Momentum in Quantum Mechanics* (Princeton University Press, Princeton, 1957).
- ²³I. C. Bowater, J. M. Brown, and A. Carrington, *Proc. Roy. Soc. London, Ser. A* **333**, 265 (1973).
- ²⁴J. M. Brown and T. J. Sears, *J. Mol. Spectrosc.* **75**, 111 (1979).
- ²⁵K. Yamada, *J. Mol. Spectrosc.* **81**, 139 (1980).
- ²⁶K. Yokoyama, W. C. Lineberger, and K. M. T. Yamada, *J. Mol. Spectrosc.* **178**, 93 (1996).
- ²⁷J. M. Virtilek, C. A. Gottlieb, E. W. Gottlieb, T. C. Killian, and P. Thaddeus, *Astrophys. J.* **364**, L53 (1990).
- ²⁸S. Saito, S. Yamamoto, W. M. Irvine, L. M. Ziurys, H. Suzuki, M. Ohishi, and N. Kaifu, *Astrophys. J.* **334**, L113 (1988).
- ²⁹T. Oka and Y. Morino, *J. Mol. Spectrosc.* **6**, 472 (1961); W. Gordy and R. L. Cook, *Microwave Molecular Spectra. Techniques of Chemistry* (Wiley, New York, 1984), Vol. 18.
- ³⁰C. A. Gottlieb, T. C. Killian, P. Thaddeus, P. Botschwina, J. Flügge, and M. Oswald, *J. Chem. Phys.* **98**, 4478 (1993).
- ³¹U. Fano, *Phys. Rev.* **124**, 1866 (1961).
- ³²D. C. Clary, *J. Phys. Chem.* **92**, 3173 (1988).
- ³³J. Simons, *J. Chem. Phys.* **91**, 6858 (1989).
- ³⁴R. S. Berry, *J. Chem. Phys.* **45**, 1228 (1966).
- ³⁵E. S. Chang and U. Fano, *Phys. Rev. A* **6**, 173 (1972); C. H. Greene and Ch. Jungen, *Adv. At. Mol. Phys.* **21**, 51 (1985).
- ³⁶H. R. Sadeghpour and C. H. Greene, *Phys. Rev. Lett.* **65**, 313 (1990).
- ³⁷J. A. Stephens and C. H. Greene, *Phys. Rev. Lett.* **72**, 1624 (1994).